NANO LETTERS

Letter

pubs.acs.org/NanoLett

Plasmonic Properties of Gold Nanoparticles Separated from a Gold Mirror by an Ultrathin Oxide

Syed Mubeen,[†,∥] Shunping Zhang,[§,∥] Namhoon Kim,[†] Seungjoon Lee,[†] Stephan Krämer,[‡] Hongxing Xu,[§] and Martin Moskovits*[,†]

[†]Department of Chemistry and Biochemistry and [‡]Materials Department, University of California, Santa Barbara, California 93106, United States

[§]Nanoscale Physics and Devices Laboratory, Institute of Physics, Chinese Academy of Sciences, ZhongGuanCun, Beijing 100190, People's Republic of China

Supporting Information

ABSTRACT: That a nanoparticle (NP) (for example of gold) residing above a gold mirror is almost as effective a surface enhanced Raman scattering (SERS) substrate (when illuminated with light of the correct polarization and wavelength) as two closely coupled gold nanoparticles has been known for some time.[1,2] The NP-overmirror (NPOM) configuration has the valuable advantage that it is amenable to top-down fabrication. We have fabricated a series of Au-NPOM substrates with varying but thin atomic layer-deposited oxide spacer and measured the SERS enhancement as a function of spacer thickness and angle of incidence (AOI). These were compared with high-quality finite-difference time-domain calculations, which reproduce the observed spacer thickness and AOI dependences faithfully. The SERS intensity is expected to be strongly affected by the AOI on account for the fact that the hot spot formed in the space between the NP and the mirror is most efficiently excited with an electromagnetic field component that is normal to the surface of the mirror. Intriguingly we find that the SERS intensity maximizes at ~60° and show that this is due to the coherent superposition of the incident and the reflected field components.[3] The observed SERS intensity is also shown to be very sensitive to the dielectric constant of the oxide spacer layer with the most intense signals obtained when using a low dielectric constant oxide layer (SiO_2).

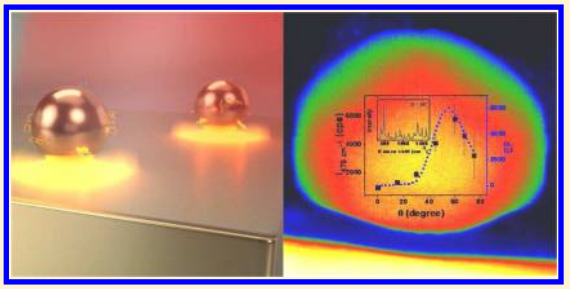

KEYWORDS: *Surface plasmons, nanoparticles, gold mirror, dielectric layer, near-field coupling, SERS*

Surface-enhanced Raman scattering (SERS) is an extensively studied, label-free spectroscopic technique for obtaining molecule-specific information. The SERS enhancement arises from the concentration of the local electromagnetic (EM) fields near appropriately nanostructured metal systems resulting from localized surface plasmon excitations. For excitation in or near the visible portion of the spectrum the effect is most pronounced in gold and silver (and, for completeness, the alkalis).[4−7] It is now almost universally acknowledged that the largest contributions to SERS arise from molecules located in nanogaps or clefts where the electromagnetic field enhancement is especially concentrated. Under favorable circumstances the field concentration is sufficient to enable the detection of a single molecule.[8−10]

A large array of SERS substrates, and materials on which SERS substrates may be based, have been developed and reported.[11−23] One of these, first proposed theoretically by Metiu,[1,2] the nanoparticle-on-mirror (NPOM) configuration in which a nanoparticle is separated from a bulk metal surface, such as a thick metal film[24−38] is the subject of this report. To a first approximation, the physics of this system is isomorphic to that of two coupled nanoparticles since the electrostatics of the charges on a metal nanoparticle located above a semi-infinite, perfectly conducting metal plane mimics the interaction of the nanoparticle with an image particle on which the charges are conjugate to those on the nanoparticle. Hence, one expects the greatest SERS enhancements to occur with light polarized along the surface normal, and the least when the light is polarized along the surface of the film[1,3] since in the latter case the dipolar component for the distribution of the charges and the image charges vanishes when the magnitudes of the image charges equal those of the original charges.

A more complete analysis treats the dynamical interactions of the localized surface plasmons (LSPs) of the nanoparticle with the surface plasmon polaritons (SPPs) supported by the underlying metal film (and takes into account the actual optical constants of the materials involved). This can lead to some interesting and complex optical effects.

The NPOM configuration is especially promising as a SERS substrate since it is compatible, at least for most of its construction, with well-developed top-down foundry processes,

Received: January 27, 2012
Revised: February 29, 2012
Published: March 13, 2012

   dx.doi.org/10.1021/nl300351j | *Nano Lett.* 2012, 12, 2088−2094

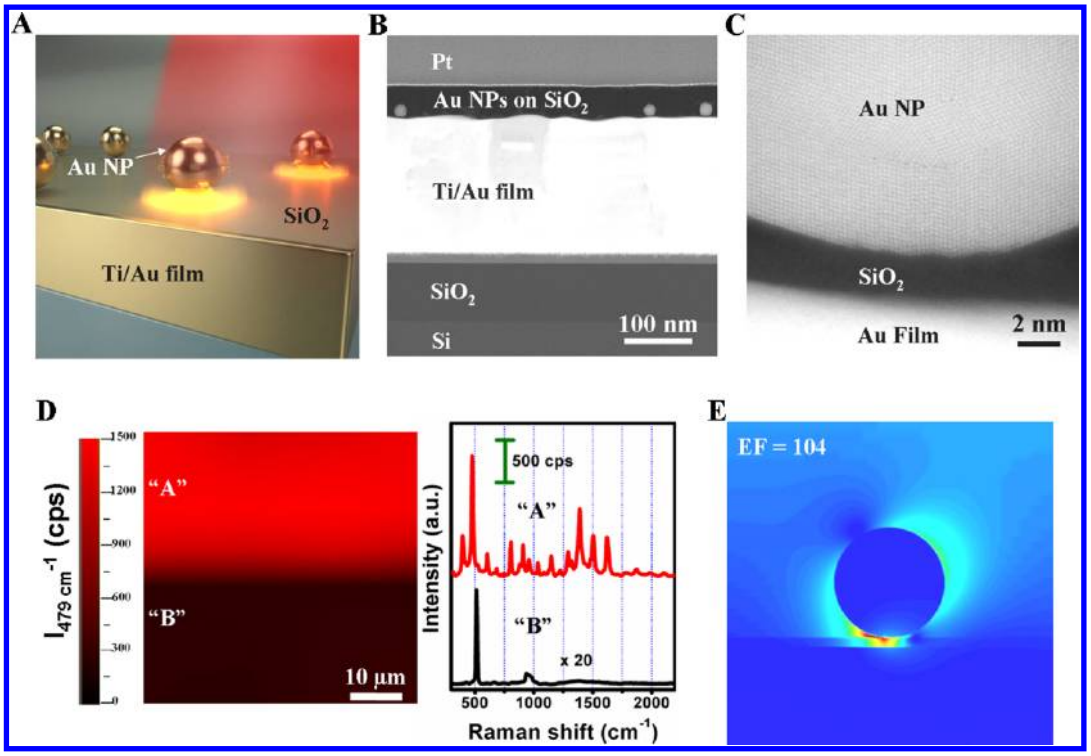

Figure 1. (A) Schematic and (B) cross sectional HAADF STEM images of Au-NP near a gold film separated by a thin dielectric spacer deposited using ALD technique. (C) High-resolution TEM image of an individual Au-NP on a 2 nm SiO_2 spacer showing its clear separation from the underlying gold film. (D) SERS spectral maps of two regions of the substrate. The first ("A") is the NPOM; the second ("B") is a region where the Au-NPs are deposited on the SiO_2/Si surface with no Au film. Representative SERS spectra of each region are shown to its right. The strong Raman line at ~520 cm^{-1} is due to Si. (E) Calculated spatial distribution of the EM field with 633 nm excitation for a Au NPOM assuming a 3 nm SiO_2 layer.

which can lead to the manufacture of large area SERS substrates with great spot-to-spot uniformity. Because the aforementioned electrodynamic interactions are critically sensitive to the distance between the nanoparticle and the mirror,[28,35,39] especially at very close distances (<~5 nm), a key issue is to develop strategies for organizing nanoparticles uniformly on a macroscopic mirror film that is covered with a very thin dielectric spacer with high structural integrity. Several strategies have been reported in the context of producing NPOM SERS substrates for laying down the dielectric spacer including surface functionalization of the metal film using a polyelectrolyte layer,[30] self-assembled molecular layers,[31,35,37] or polymer brushes.[26] Stable oxides like SiO_2 produced using conventional evaporation techniques have also been reported.[24]

In this report, we describe the fabrication of devices consisting of well-separated gold nanoparticles (Au-NPs) residing on a thin oxide spacer layer covering a gold mirror (~200 nm of gold deposited on a silicon wafer) using a combination of top-down nano and microfabrication technologies and bottom-up nanoparticle synthesis. The plasmonic properties of these devices were interrogated as a function of spacer thickness and angle of incidence (AOI) of both s- and p-polarized light, using SERS as a probe. Very thin oxide films with high structural integrity and thickness uniformity were produced using atomic layer deposition (ALD). Devices with silica (SiO_2), alumina (Al_2O_3), and zirconia (ZrO_2) spacers were fabricated. They all showed similar trends with respect to the above-mentioned variables. The substrates fabricated with silica spacer layers produced the most intense SERS signals. Accordingly, we will concentrate on those samples. Oxide thicknesses of 2 nm and above were found to have the structural integrity and uniformity required for this study.

Briefly, the fabrication process consisted of preparing a gold film on a Si/SiO_2 wafer substrate by e-beam evaporating 20 nm of Ti followed by 200 nm of gold at a deposition rate of 1 Å s^{-1}. The Au film was then coated with an oxide layer of varying thickness using ALD and the oxide-covered gold substrates were incubated in aminopropyltriethoxysilane (APTES) solution to help immobilize the AuNPs that were subsequently deposited on the oxide surface by dip-coating the substrate in an aqueous Au-NP (diameter ~30−35 nm) solution (~2 × 10^{11} particles/ml) for varying lengths of time. Dipping times in the range 5−30 s produced sufficient coverage to produce strong SERS signals yet kept the particle surface density sparse with well-separated Au-NPs. The devices produced for these studies were exposed to the Au-NP solution for ~10 s resulting in nanoparticle coverage ~4−6 Au NPs per μm^2 (see Supporting Information Figure 1). These low NP converges were purposely selected to minimize NP−NP coupling so as to restrict the plasmonic properties to those originating from the hot spots located between the Au-NPs and its underlying gold film with negligible contribution from hot spots located between neighboring Au-NPs. Of course, much stronger SERS signals could be obtained at very high NP coverages as we show below and as observed recently by Tian et al.[40] But then the substrate would lack the structural simplicity that allows us to compare measured and calculated data quantitatively. A schematic representation of the nanoparticle on mirror architecture is shown in Figure 1A. The NPOM architecture was confirmed by high-angle annular dark field

dx.doi.org/10.1021/nl300351j | Nano Lett. 2012, 12, 2088−2094

scanning transmission electron microscopy (HAADF STEM; Figure 1B,C). Figure 1B,C shows the ~2 nm thick SiO_2 spacer separating the Au-NPs and the underlying gold film, clearly.

Following their fabrication, the devices were incubated overnight in a 100 μM aqueous thionine solution, a reporter molecule with an excellent Raman cross section. The strong SERS signals observed are undoubtedly dominated by signals originating from thionine resident in the annular interstice surrounding the point of contact between the nanoparticle and the substrate (as shown in Figure 1A).

Raman spectra were recorded using a LabRam system (Horiba Jobin Yvon) equipped with 1200 grooves/mm holographic gratings and Peltier-cooled CCD detector. Continuous wave 633 nm He−Ne laser was used to excite the spectra that were collected in a backscattering geometry using a confocal Raman microscope (high stability BX40) equipped with Olympus objective. A 10× objective lens with a numerical aperture (NA) of 0.3 was used to focus the laser. The illuminating laser beam for the above NA is estimated to have an outer conical envelope for which the half angle is 15°. Angle-dependent SERS spectra were measured by attaching the substrates to a rotation stage. Measurements were taken with light polarized both in the s and p directions. In the former, the incident polarization of the laser (and of the collected light) remains in the plane of the substrate independent of the angle of incidence, while for the latter the component of light polarized normal to the substrate's surface increases with increasing angle of incidence. (Although one needs to keep in mind that the cylindrically symmetric geometry of the focal cone means that there will always be a small normal component present even for nominally s-polarized light.)

Despite the low density of particles, the SERS signals were found to be rather uniform across the sample as shown in the SERS spectral map (Figure 1D). For SERS spectra collected at 100 different locations on a single substrate (the substrate area was ~1 × 1 cm^2 and measurement area was 50 × 50 μm^2), the greatest variation in the 479 cm^{-1} SERS band intensity was found to be 9%. Figure 1D also illustrates the dramatic effect on the SERS intensity of the coupling between the Au-NPs and the underlying gold film. Region A (in Figure 1D) corresponds to an area of the substrate where the Au NP were placed above a gold mirror separated by 2 nm of SiO_2, while in region B the Au-NPs were attached to SiO_2 with no underlying gold film. No discernible SERS spectra could be detected from the NPs resident on SiO_2 without an underlying gold mirror.

It will also be evident on the basis of the computations, which we present below, that the SERS spectra observed at normal incidence (i.e., with the electric vector of the incident laser ostensibly polarized in the plane of the substrate) in region A are preponderantly due to the small component of light polarized normal to the substrate's surface arising from the conical geometry of the focused laser beam. In fact, for illumination with light strictly polarized tangential to the metal surface the coupling between the Au-NP and the metal surface actually results in a lower level of overall enhancement than for an isolated NP. This is because the dynamics of system consisting of the light-induced dipole on the Au-NP plus that due to its charge-conjugate image have the overall symmetry of a quadruple. In contrast, for an incident field polarized normal to the metal surface the electrodynamic interactions between the LSP of the Au NP and the metallic film produce a system with a strong overall dipole wherein the electromagnetic fields are concentrated in a hot spot in the vicinity of the space between the Au-NP and the Au film.

To better understand the plasmon couplings in the NPOM system, full wave electromagnetic simulations were performed using finite-difference time-domain (FDTD) software (Lumerical FDTD Solution 7.5.1). The sample geometries assumed in the calculations closely matched those of the actual samples, that is, a 35 nm Au-NP sitting on a 200 nm thick Au film was assumed with a dielectric spacer of varying thickness and dielectric constant in between. The silicon substrate was also included, and the computation domain was truncated by a perfectly matched layer to mimic a situation in which the air above the sample and the Si substrate were infinite. The excitation source was assumed to be a linearly polarized plane wave. A mesh of 0.25 nm was used that ensured the validity of field enhancement in the vicinity of the hot-spot. The optical constants of gold and silicon were taken from ref 4 and ref 41, respectively. In all of the simulations, the measured enhancement factor (EF) was assumed to be proportional to the fourth power of the modulus of the computed fields and averaged over a surface 1 nm above the Au-NP's surface where the molecules were assumed to reside (see Supporting Information Figure 2). And although the adsorbed molecules likely cover the nanoparticle uniformly and fill the interstices to the extent that they can, the SERS signals arise disproportionately from the annular hot-spot region between the NP and the oxide.

Figure 1E shows the calculated EM field for a Au-NPOM with a 3 nm silica spacer layer illuminated with 633 nm laser light. A p-polarized laser beam illuminating the system at an AOI of 15° simulated the 15° focal cone corresponding to the numerical aperture used. (All calculations simulating normal incidence were actually carried out at an AOI of 15° to account for the focal cone of the illuminating laser. For AOI values greater than 15° no correction for the focal cone was made or necessary, since the effect of the field component normal to the Au film's surface greatly exceeded the effect due to the finite optical aperture.) The strongest EM fields in the hot spot region result from the small incident field component polarized normal to the gold film surface. The enhanced field strength appears to be suddenly compressed on passing from the region of space between the NP and the oxide into the interior of the oxide spacer. This is a manifestation of Maxwell's continuity conditions, which require the normal component of the electric displacement ($\vec{D} = \varepsilon\vec{E}$) to be continuous across the interface between two materials. Accordingly, on passing from the oxide to air the normal component of the electric field strength in air will be larger than its value in the oxide by a factor approximately equal to the dielectric constant of the oxide. This gives the impression that the hot spot is compressed in size in the oxide as compared to the region between the oxide and the NP.

Also, with illumination at 15° AOI the hot spot seems a little asymmetric. This is because at such small angles of incidence, the normal component of the incident field is of the same order of magnitude as the tangential component, so that the field component excited in the NP by the tangential component which is slightly tilted from the poles of the NP on account of the direction of the wave vector of the incident light can compete successfully with the field due to the normal component, resulting in the observed asymmetry.

As the AOI increases, the tangential field component in the hot spot region can no longer compete efficiently with the normal component (Figure 2) causing the distribution of

dx.doi.org/10.1021/nl300351j | Nano Lett. 2012, 12, 2088−2094

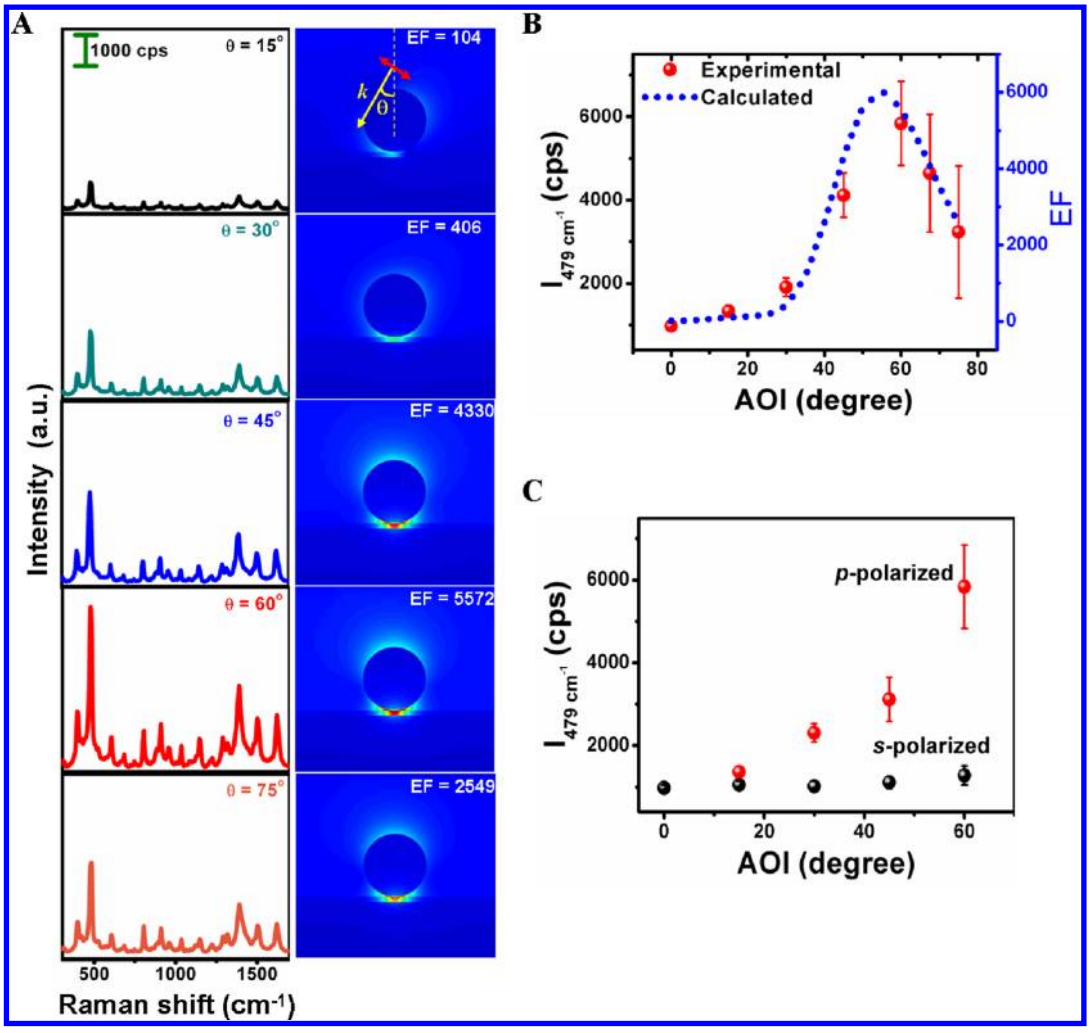

Figure 2. Effect of angle of incidence for p-polarized laser excitation on (A) the measured SERS spectra and it is corresponding calculated EM field distribution and enhancement factors for a gold NPOM with 3 nm SiO_2 thickness. (B) Averaged SERS intensities for the 479 cm^{-1} compared with calculated EM field enhanced factors for different incident angle. (C) Response of SERS intensities to polarization of the incident beam.

enhanced field values in the region of the hot spot to become progressively more symmetric.

Hence our observations accord completely with the computations. For the single NPOM configuration, the SERS intensity is dominated by the normal polarization component, which at normal incidence arises entirely from the conical shape of the focused beam (with, for the numerical aperture used has a cone half angle of 15°). For AOI values greater than ~20°, the much larger incident field component polarized along the surface is predicted to contribute negligibly in contrast to the normal field component.

Figure 2 shows the effect of angle of incidence dependence on illuminating a NPOM system fabricated with a 3 nm SiO_2 spacer for both s- and p-polarized light. For p-polarized excitation (and collection) the SERS intensity initially increases with increasing angle of incidence reaching a maximum value when the AOI is ~60° (Figure 2A). With further increase AOI, the SERS intensity decreases. This maximum arises from the fact that the EM field at a given point above a mirror can be considered to be a coherent superposition of the EM field for the light ray directly illuminating that point plus that for a ray that is reflected from the surface. For p-polarized light the phase difference between the field components of the incident and reflected rays changes by π-radians at the principle angle (which for gold occurs at ~60°) producing this maximum. For AOI values below the principle angle, the SERS intensity increases as the AOI increases because the field component normal to the substrate's surface increases and the field component of the direct beam adds to the field component of the reflected beam. Beyond that angle, the magnitude of the normal field component continues to increase; however, the change in phase of the reflected beam now causes it to subtract from the field component of the direct beam. This result is isomorphic with what was predicted for p-polarized spectroscopy of a molecule above a silver surface.[3]

This effect is faithfully reproduced in the calculated EM field images that show stronger confinement of the fields with increasing angle of incidence for p-polarized light reaching a maximum at ~55° (Figure 2A,B). No such dependence is expected nor was it observed with s polarization (Figure 2C). Thus the optimal experimental configuration to ensure maximum SERS activity for NP on mirror configuration is to position the incident beam at ~60° to the substrate surface normal. One way to accomplish this is to create a substrate that consists of pyramids or pyramidal pits whose sides slope at 60°, rather than on a plane substrate.

The ability of ALD to produce oxide film thicknesses of high precision allowed us to investigate the spacer layer dependence

dx.doi.org/10.1021/nl300351j | Nano Lett. 2012, 12, 2088−2094

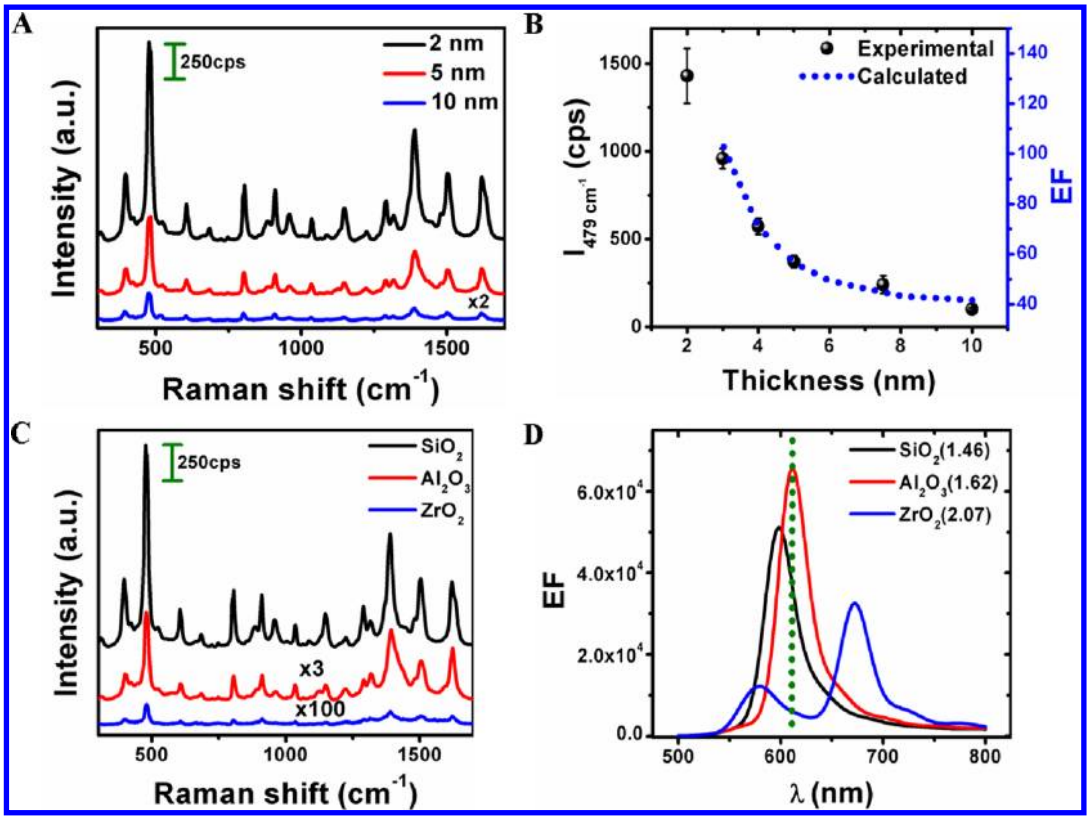

Figure 3. (A) Representative SERS spectra of thionine excited with 633 nm for a Au NPOM as a function of SiO_2 layer thickness. (B) Averaged intensities for the 479 cm^{-1} SERS band compared with calculated EM field enhanced factors for varying SiO_2 layer thickness. Other peaks in the SERS spectrum show identical trends. (C) SERS spectra obtained at normal incidence for NPOMs fabricated with 2 nm thick spacer layers composed of one of three metal oxides: SiO_2, which has the lowest dielectric constant, followed by Al_2O_3 and ZrO_2. (D) Calculated EFs for NPOMs with 2 nm layers of different dielectrics (their corresponding refractive index shown in the inset), as a function of excitation wavelength. The calculations were carried out assuming 45° AOI.

of the electromagnetic film concentrated in the annular gap surrounding the point of contact between an Au-NP and the oxide, assuming that the SERS signals originated primarily from molecules residing in that region. This trend could then be compared to what calculations predict. Ellipsometric measurements were performed on witness samples to determine the relationship between the oxide thickness and the number of ALD deposition cycles. The relationship was found to be proportional (see Supporting Information Figure 3), consistent with previous studies.[42,43] The SERS spectra obtained for varying SiO_2 thickness at normal incidence are shown in Figure 3A. The spectrum agrees well with previously reported spectra of thionine.[44] Not unexpectedly, the SERS intensity drops significantly on increasing the silica film thickness from 2 to 10 nm (Figure 3A,B). The trend in the enhancement versus oxide layer thickness matches the enhancement factors calculated using FDTD very satisfactorily (Figure 3B).

Although the electrostatic picture of a metal nanoparticle resident on a metal mirror has some elements in common with a system of two interacting metal nanoparticles, there are also some seminal differences. Some of these are trivial. For example, the image particle is not in general perfectly complementary to the actual nanoparticle because the metal mirror is not a perfect conductor. Less trivially, the time-varying dipole induced in the junction at the metal NP/mirror interface can launch SPPs that can propagate outward as circular waves along the interface and contribute to the electromagnetic fields resident in the NP-mirror hot spot of neighboring NPs when it crosses those points, and even at the original launch point when the SPP reflects back from the film's edge or is secondarily scattered from sites where other NPs reside. The contribution of these processes can be quite complex since the various propagating waves can result from multiple scattering events that add coherently, and their amplitudes diminish with propagation distance both on account of intrinsic losses and because the energy is distributed over expanding circular wavefronts.

Hence, the SERS enhancement observed for molecules resident in the cleft between the Au-NP and oxide film can be broadly viewed as originating from the following two contributions: (1) the electromagnetic field associated with the incident laser light that excites the gap modes at the site of the NP-surface junction that functions as an antenna concentrating radiant energy in the gap where molecules reside (the electrostatic part); and (2) the electromagnetic energy concentrated at that junction derived from SPPs, which are also excited in step 1, that then propagate outward and couple energy into the junctions of neighboring NP-mirror sites. Since the illumination is CW, the energy in the polaritons can build up to a significant level until the rate of energy infusion equals the rate of energy losses.

We believe that the first effect, namely the electromagnetic energy concentration in the hot spot formed between the Au-NP and the underlying gold mirror will be the dominant contribution on account of the aforementioned loss mechanisms affecting the propagating SPPs. Hence, the simulation

dx.doi.org/10.1021/nl300351j | Nano Lett. 2012, 12, 2088−2094

approach we used in this report is expected to describe our observations adequately.

The simulations reproduce the observed angle-of-incidence behavior of the SERS intensity and the effect of oxide thickness very well. The only observation that is not predicted entirely correctly is the dependence on the dielectric constant of the oxide spacer. Three materials were used to fabricate the spacer: SiO_2, Al_2O_3, and ZrO_2, whose reported dielectric constants (at optical frequencies) are, respectively, 2.1, 2.6, and 4.3.[45−47] The observed SERS intensities at all of the spacer thicknesses used were greatest for SiO_2, less intense for alumina and very much less intense for zirconia. For substrates fabricated with 2 nm spacer layers, the SERS intensity was found to be 7-fold more intense with a spacer layer of SiO_2 than that with Al_2O_3 for 633 nm illumination. The SERS intensity decreased even more with ZrO_2 spacers (Figure 3C).

The calculations predict a rather complex dielectric constant behavior that depends sensitively on the spacer layer thickness, the diameter of the NP and also the location within the cleft formed by the NP resting on oxide layer where the molecules might be located. For example, for a 2 nm spacer layer at 45° AOI, and values for the other parameters as given in the caption of Figure 3D, the SERS intensity with 633 nm laser excitation is predicted to have approximately twice the intensity with an alumina spacer as with a silica spacer (the observations showed the reverse order), while with the zirconia spacer the SERS intensity was calculated to be ∼50-fold smaller, which is more or less as observed. A clue to explaining the discrepancy between what is observed with silica and alumina and what is calculated might be the rather narrow resonances calculated for wavelength dependence of the fields concentrated in the hot spots. This means that rather small variations in the dielectric constant values of the spacer layers, or in the size of the cleft (due, for example, to lack of perfect sphericity of the NP) could easily reverse the order of SERS intensities for observed for silica and alumina whose dielectric constants do not vary greatly but would correctly predict the behavior with zirconia spacers, whose dielectric constant is significantly larger.

A set of experiments were carried out as a function of Au-NP coverage on substrates consisting of 5 nm SiO_2 covered Au films by changing the immersion time of the substrates in the gold colloid solution, while keeping all other parameters constant. As shown in Figure 4, the SERS intensity increases almost linearly for NPOMs with increasing particle coverage when the particle densities were low enough for the Au-NPs to remain isolated. No observable SERS signal was obtained for an equal number of isolated AuNPs on substrates without the Au mirror. Prolonged exposure to Au-NPs (1 min), however, produced substrates with dramatically increased SERS activity. Moreover, strong SERS signals were observed both from the region with and without the Au mirror. This was attributed to the formation of Au NP dimers and higher aggregates (see inset Figure 4), which create hot spots between nanoparticle aggregates oriented appropriately for excitation with s-polarized light even at normal incidence. However, the SERS intensity measured from the NPOM region was 10-fold greater than in the absence of the mirror even for substrates dominated by Au dimers and larger aggregates for which the hot spots are disposed appropriately for excitation by s-polarized light. This possibly implies that for 2D nanoparticle aggregates residing above a mirror the hot spot residing between the particle and the mirror that can normally only be excited with a field component normal to the mirror surface will now also be excitable with s-polarized light likely due to the (diagonal) cross-coupling between nanoparticles and the images of neighboring nanoparticles in addition to the normal coupling that occurs between nanoparticles in dimers or aggregates and between a given nanoparticle and its own image.

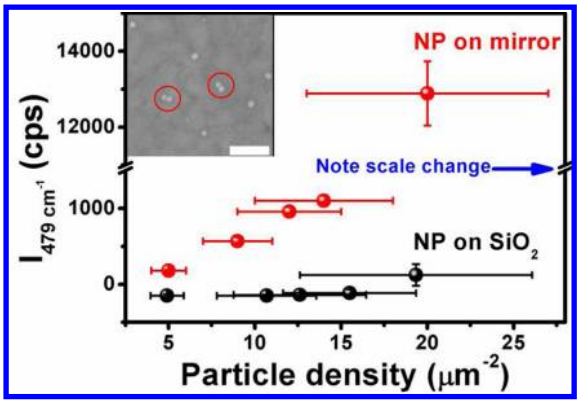

Figure 4. Effect of Au-NP particle density (varied by varying the dipping time) on the SERS intensity of Au NPOMs fabricated with 5 nm SiO_2 spacers. With a dipping time of 1 min (and greater), Au-NP dimers and trimers were observed. (See SEM image in the inset; scale bar = 200 nm.) Note the scale break in the *y*-axis that affects the last point.

In conclusion, NPOMs fabricated with very thin ALD-deposited spacer layers are SERS substrates with highly reproducible and uniform SERS activity. Their physical properties are excellently predicted using full-wave electromagnetic field calculations based on FDTD. When using p-polarized light and an angle of incidence ∼60°, these substrates produce very high SERS enhancements even for Au-NPs that are isolated from one another. Au-NP aggregates, which show very intense SERS signals on their own, still benefit from the presence of an underlying Au mirror by enhancement factors ∼10. Finally, these systems can be reproducibly and scalably fabricated since many of the steps are compatible with well established and low-cost wafer processing technologies.

■ ASSOCIATED CONTENT

Ⓢ Supporting Information

SEM and corresponding histograms of Au-NP density, schematic diagram of the integral surface used for the calculations and ALD cycle versus spacer thickness dependence. This material is available free of charge via the Internet at http://pubs.acs.org.

■ AUTHOR INFORMATION

Corresponding Author

*E-mail: moskovits@chem.ucsb.edu.

Author Contributions

‖These authors contributed equally to the work

Notes

The authors declare no competing financial interest.

■ ACKNOWLEDGMENTS

The authors thank Gary Braun and Allessia Pallaoro for technical support and Peter Allen for graphic support. This work was supported by the Institute for Energy Efficiency, an Energy Frontier Research Center funded by the U.S. Department of Energy, Office of Science, Office of Basic Energy Sciences, Award Number DE-SC0001009. We also

gratefully acknowledge support from the Institute for Collaborative Biotechnologies through Grant DAAD19-03-D-0004 from the U.S. Army Research Office. We also made extensive use of the MRL Central Facilities at UCSB supported by the National Science Foundation under Award Nos. DMR-0080034 and DMR-0216466 for the HRTEM/STEM microscopy.

REFERENCES

(1) Aravind, P. K.; Rendell, R. W.; Metiu, H. *Chem. Phys. Lett.* **1982**, *85* (4), 396−403.
(2) Aravind, P. K.; Metiu, H. *J. Phys. Chem.* **1982**, *86* (26), 5076−5084.
(3) Moskovits, M. *J. Chem. Phys.* **1982**, *77* (9), 4408−4416.
(4) Johnson, P. B.; Christy, R. W. *Phys. Rev. B* **1972**, *6* (12), 4370−4379.
(5) Zeman, E. J.; Schatz, G. C. *J. Phys. Chem.* **1987**, *91* (3), 634−643.
(6) Moskovits, M. *J. Raman Spectrosc.* **2005**, *36* (6−7), 485−496.
(7) Ford, M. J.; Blaber, M. G.; Arnold, M. D.; Harris, N.; Cortie, M. B. *Physica B* **2007**, *394* (2), 184−187187.
(8) Kneipp, K.; Wang, Y.; Kneipp, H.; Perelman, L. T.; Itzkan, I.; Dasari, R.; Feld, M. S. *Phys. Rev. Lett.* **1997**, *78* (9), 1667−1670.
(9) Xu, H. X.; Bjerneld, E. J.; Käll, M.; Börjesson, L. *Phys. Rev. Lett.* **1999**, *83* (21), 4357−4360.
(10) Moskovits, M.; Tay, L. L.; Yang, J.; Haslett, T. 10. SERS and the single molecule. In *Optical Properties of Nanostructured Random Media*; Springer-Verlag: Berlin, 2002; Vol. *82*, pp 215−226.
(11) Freeman, R. G.; Grabar, K. C.; Allison, K. J.; Bright, R. M.; Davis, J. A.; Guthrie, A. P.; Hommer, M. B.; Jackson, M. A.; Smith, P. C.; Walter, D. G.; Natan, M. J. *Science* **1995**, *267* (5204), 1629−1632.
(12) Dick, L. A.; McFarland, A. D.; Haynes, C. L.; Van Duyne, R. P. *J. Phys. Chem. B* **2002**, *106* (4), 853−860.
(13) Tian, Z. Q.; Ren, B.; Wu, D. Y. *J. Phys. Chem. B* **2002**, *106* (37), 9463−9483.
(14) Tao, A.; Kim, F.; Hess, C.; Goldberger, J.; He, R. R.; Sun, Y. G.; Xia, Y. N.; Yang, P. D. *Nano Lett.* **2003**, *3* (9), 1229−1233.
(15) Chaney, S. B.; Shanmukh, S.; Dluhy, R. A.; Zhao, Y. P. *Appl. Phys. Lett.* **2005**, *87* (3), 3.
(16) Lu, Y.; Liu, G. L.; Lee, L. P. *Nano Lett.* **2005**, *5* (1), 5−9.
(17) Talley, C. E.; Jackson, J. B.; Oubre, C.; Grady, N. K.; Hollars, C. W.; Lane, S. M.; Huser, T. R.; Nordlander, P.; Halas, N. J. *Nano Lett.* **2005**, *5* (8), 1569−1574.
(18) Schierhorn, M.; Lee, S. J.; Boettcher, S. W.; Stucky, G. D.; Moskovits, M. *Adv. Mater.* **2006**, *18* (21), 2829.
(19) Zhang, X. Y.; Zhao, J.; Whitney, A. V.; Elam, J. W.; Van Duyne, R. P. *J. Am. Chem. Soc.* **2006**, *128* (31), 10304−10309.
(20) Ward, D. R.; Grady, N. K.; Levin, C. S.; Halas, N. J.; Wu, Y. P.; Nordlander, P.; Natelson, D. *Nano Lett.* **2007**, *7* (5), 1396−1400.
(21) Le, F.; Brandl, D. W.; Urzhumov, Y. A.; Wang, H.; Kundu, J.; Halas, N. J.; Aizpurua, J.; Nordlander, P. *ACS Nano* **2008**, *2* (4), 707−718.
(22) Banholzer, M. J.; Millstone, J. E.; Qin, L. D.; Mirkin, C. A. *Chem. Soc. Rev.* **2008**, *37* (5), 885−897.
(23) Deng, X. G.; Braun, G. B.; Liu, S.; Sciortino, P. F.; Koefer, B.; Tombler, T.; Moskovits, M. *Nano Lett.* **2010**, *10* (5), 1780−1786.
(24) He, L.; Smith, E. A.; Natan, M. J.; Keating, C. D. *J. Phys. Chem. B* **2004**, *108* (30), 10973−10980.
(25) Tokareva, I.; Minko, S.; Fendler, J. H.; Hutter, E. *J. Am. Chem. Soc.* **2004**, *126* (49), 15950−15951.
(26) Daniels, J. K.; Chumanov, G. *J. Phys. Chem. B* **2005**, *109* (38), 17936−17942.
(27) Kim, K.; Yoon, J. K. *J. Phys. Chem. B* **2005**, *109* (44), 20731−20736.
(28) Anderson, D. J.; Moskovits, M. *J. Phys. Chem. B* **2006**, *110* (28), 13722−13727.
(29) Kinnan, M. K.; Chumanov, G. *J. Phys. Chem. C* **2007**, *111* (49), 18010−18017.
(30) Mock, J. J.; Hill, R. T.; Degiron, A.; Zauscher, S.; Chilkoti, A.; Smith, D. R. *Nano Lett.* **2008**, *8* (8), 2245−2252.
(31) Rodríguez-Lorenzo, L.; Álvarez-Puebla, R. A.; Pastoriza-Santos, I.; Mazzucco, S.; Stéphan, O.; Kociak, M.; Liz-Marzán, L. M.; de Abajo, F. J. G. *J. Am. Chem. Soc.* **2009**, *131* (13), 4616.
(32) Wang, K.; Schonbrun, E.; Crozier, K. B. *Nano Lett.* **2009**, *9* (7), 2623−2629.
(33) Yoon, I.; Kang, T.; Choi, W.; Kim, J.; Yoo, Y.; Joo, S. W.; Park, Q. H.; Ihee, H.; Kim, B. *J. Am. Chem. Soc.* **2009**, *131* (2), 758−762.
(34) Chen, S. Y.; Mock, J. J.; Hill, R. T.; Chilkoti, A.; Smith, D. R.; Lazarides, A. A. *ACS Nano* **2010**, *4* (11), 6535−6546.
(35) Hill, R. T.; Mock, J. J.; Urzhumov, Y.; Sebba, D. S.; Oldenburg, S. J.; Chen, S. Y.; Lazarides, A. A.; Chilkoti, A.; Smith, D. R. *Nano Lett.* **2010**, *10* (10), 4150−4154.
(36) Liu, Y.; Xu, S. P.; Li, H. B.; Jian, X. G.; Xu, W. Q. *Chem. Commun.* **2011**, *47* (13), 3784−3786.
(37) Liu, B.; Blaszczyk, A.; Mayor, M.; Wandlowski, T. *ACS Nano* **2011**, *5* (7), 5662−5672.
(38) Yamamoto, N.; Ohtani, S.; de Abajo, F. J. G. *Nano Lett.* **2011**, *11* (1), 91−95.
(39) Chu, Y. Z.; Banaee, M. G.; Crozier, K. B. *ACS Nano* **2010**, *4* (5), 2804−2810.
(40) Li, J. F.; Ding, S. Y.; Yang, Z. L.; Bai, M. L.; Anema, J. R.; Wang, X.; Wang, A.; Wu, D. Y.; Ren, B.; Hou, S. M.; Wandlowski, T.; Tian, Z. Q. *J. Am. Chem. Soc.* **2011**, *133* (40), 15922−15925.
(41) Palik, E. D. *Handbook of Optical Constants of Solids*; Academic Press: New York, 1985; pp xviii, 804.
(42) Du, Y.; Du, X.; George, S. M. *Thin Solid Films* **2005**, *491* (1−2), 43−53.
(43) Dingemans, G.; van Helvoirt, C. A. A.; Pierreux, D.; Keuning, W.; Kessels, W. M. M. *J. Electrochem. Soc.* **2012**, *159* (3), H277−H285.
(44) Ruan, C. M.; Eres, G.; Wang, W.; Zhang, Z. Y.; Gu, B. H. *Langmuir* **2007**, *23* (10), 5757−5760.
(45) Ghosh, G. *Opt. Commun.* **1999**, *163* (1−3), 95−102.
(46) Chávez-Ramírez, J.; Aguilar-Frutis, M.; García, M.; Martínez, E.; Álvarez-Fregoso, O.; López, S.; Burillo, G.; Falcony, C. *Surf. Rev. Lett.* **2002**, *9* (5−6), 1637−1640.
(47) Jerman, M.; Qiao, Z. H.; Mergel, D. *Appl. Opt.* **2005**, *44* (15), 3006−3012.